Energy Reports 6 (2020) 70–76

Contents lists available at ScienceDirect

Energy Reports

journal homepage: www.elsevier.com/locate/egyr

Review article

Ion irradiation-induced foams in antimonide binary alloys: A combination of small energy bandgap with giant surface-to-bulk ratio

Raquel Giulian *, Charles A. Bolzan, Josiane Bueno Salazar, Carlo Requião da Cunha

Instituto de Física, Universidade Federal do Rio Grande do Sul, Porto Alegre – RS, Brazil

ARTICLE INFO

Article history:
Received 11 June 2019
Received in revised form 22 August 2019
Accepted 17 September 2019
Available online 24 September 2019

Keywords:
Antimonide films
Ion irradiation
XRD
SEM

ABSTRACT

This is a short review about the ion irradiation-induced foams in antimonide films. III–V semiconductors like InSb and GaSb can be transformed into solid foams with nanometric dimensions upon irradiation with swift heavy ions, increasing significantly the effective surface area of the material. The giant surface-to-bulk ratio of solid nanofoams, combined with the small energy bandgap of antimonide binary compounds offer new possibilities for the development of electronic devices with improved energy efficiency. The characterization of antimonide nanofoams structure, composition and electronic properties is thus essential to fully exploit their promising technological advantages. Here we show that InSb and GaSb films deposited by magnetron sputtering on SiO_2/Si substrates can be rendered porous upon irradiation with 17 MeV Au^{+7} ions, while no evidence of porosity was observed in AlSb films irradiated under similar conditions. InSb films initially amorphous, become polycrystalline with zincblende phase upon irradiation with fluence $2x10^{14}$ cm^{-2}, at the same time as the accumulation of voids result in the complete transformation of the films from compact-continuous to foam-like structure. Single-crystalline InSb films can also be transformed into solid foams upon irradiation, however, the ion fluence required to attain similar levels of porosity (compared to amorphous InSb deposited by magnetron sputtering) is significantly higher. GaSb films, in a similar way, can also be transformed into solid foams upon irradiation, although, for GaSb films deposited by magnetron sputtering, the structure of the foams is amorphous with significant increase of oxide fraction upon irradiation. The ion irradiation effects on the electronic properties of single crystalline InSb films are also presented. We compare the ion irradiation effects in different antimonide binary compounds with results about their crystalline structure and morphology using X-ray diffraction analysis and scanning electron microscopy.

Contents

1. Why porous antimonides are interesting

The discovery of luminescent microporous Si triggered considerable interest in porous semiconductors. Since porosity breaks the symmetry of the host lattice, the properties of porous semiconductors can be radically different from those of bulk material. Not only prime semiconductor parameters like absorption/emission of light, conductivity and bandgap might be quite different, but also high-order effects, internal symmetries/anisotropies and even basic chemistry (Foll et al., 2005). Porous semiconductors can be highly attractive from a sensor point of view, given their unique combination of crystalline structure and large internal surface area, which enables enhancement of the adsorbate effects and high activity in surface chemical

* Corresponding author.
E-mail address: raquel.giulian@ufrgs.br (R. Giulian).

https://doi.org/10.1016/j.egyr.2019.09.059

reactions. Various studies show that optical and electrical characteristics of porous semiconductors may change significantly upon adsorption of molecules to their surfaces or by filling up the pores (Korotcenkov and Cho, 2010).

Recently, porous semiconductors other than Si have received considerable attention, the most noteworthy being III–V compound materials (Datta and Som, 2016; Nitta et al., 2010; Danilov et al., 2005). These compounds offer much more possibilities in this respect as compared with Si, due to the fact that the shift from elementary to compound semiconductors entails a major crystallographic modification and offers the possibility to change their chemical composition (Vurgaftman et al., 2001). For example, by combining Al with GaAs at certain proportions, different semiconductors are obtained with different electronic bandgaps. Consequently, the properties of each of these "mixtures" can be extended by making them porous. Thus, this multitude of materials in their bulk and porous form opens the way for new exciting physical properties.

Pores in III–V compounds are not a new discovery, just as pores in Si pre-date 1990. However, much progress has been made during the last 10 years, especially the formation of pores on antimonides by ion irradiation (Nitta et al., 2010; Kluth et al., 2006; Datta et al., 2014; Jacobi et al., 2012; Kluth et al., 2011; Yanagida et al., 2017; Giulian et al., 2017b; Kluth et al., 2014a, 2005; Giulian et al., 2019). Antimonide nanofoams produced by ion irradiation exhibit smaller dimensions than nanowires grown by chemical vapour deposition, for example Anandan et al. (2019), resulting in significantly greater surface-to-bulk ratio. Moreover, Antimonide-based semiconductors are good candidates for thermoelectric materials, high speed and low power consumption electronic devices. Such properties are greatly pursued for the development of digital and analogical systems for data processing, imaging, communication and sensing, especially in portable equipment and satellites (Korotcenkov and Cho, 2010; Cheng et al., 2017). This paper will focus on more recent developments in AlSb, InSb and GaSb films deposited by magnetron sputtering, transformed into nanometric solid foams by ion irradiation. The formation of nanoporous structures in single crystalline InSb films grown by molecular beam epitaxy is also presented for comparison and the structural and electronic characterization of the films are discussed. Results about sputter-deposited films were compiled from previous publications (Giulian et al., 2017b, 2019, 2017a; Manzo et al., 2019), but we also included new results to compare the ion irradiation effects on single crystalline InSb films, for which the electrical characterizations have been performed.

2. Antimonide films: deposition and irradiation

Magnetron sputtering is a versatile technique mostly used for thin film deposition, allowing a good control of film thickness, composition and structure on a variety of structures (Giulian et al., 2017a). For the present study, we deposited AlSb, GaSb and InSb films on SiO_2/Si substrates, with thickness varying from 75 nm to 500 nm. Experimental parameters are described in detail elsewhere (Giulian et al., 2017a). For simplicity, from here on sputter-deposited films will be denoted InSb-sputt, GaSb-sputt and AlSb-sputt.

After deposition, samples were irradiated with 17 MeV Au^{7+} ions at fluences varying from 1×10^{12} to 1×10^{15} cm^{-2}. Irradiations were performed at room temperature, with the ion beam parallel to the samples normal. Further details about irradiation conditions can be seen in Refs. Giulian et al. (2017b,a). Single-crystalline InSb films, ∼370 nm thick, epitaxially grown on semi-insulating GaAs substrates by molecular beam epitaxy (MBE) were also irradiated with same energy and fluence, and the results are presented here for comparison. For clarity, films grown by MBE will be denoted InSb-MBE from here on. Scanning electron microscopy (SEM) and X-ray diffraction (XRD) analyses were performed before and after irradiation (experimental details described elsewhere (Giulian et al., 2017b, 2019, 2017a)).

The carrier mobility and density for InSb-MBE were estimated via Van der Pauw/Hall measurements. A magnetic field of 3280 Gauss was applied perpendicular to the sample and a current smaller than 1 mA was used in all measurements.

3. Ion irradiation-induced foams

When energetic heavy ions pass through a solid, the ions lose energy to the electrons and nuclei of the material along their trajectory. In the nuclear stopping regime (S_n) the impinging ions create damaged regions approximately spherical, most prominent at the end of trajectory, while in the electronic stopping regime (S_e) the energy transferred to the electrons usually results in ion track formation, of cylindrical shape, along the ion path (Toulemonde et al., 2006). In both cases, the energy lost by the impinging ions yields an increase in the local atomic motion around the ion path (S_e) or at the end of trajectory (S_n), equivalent to a local increase in temperature. For a short time, the local temperature may exceed that required for melting or even vaporization of the material and is rapidly dissipated. Despite their very different mechanisms, both S_e and S_n result in highly damaged regions that originate from a quench from the melt, but with different shapes. For this reason, it is expected that both S_n and S_e result in porous structures with similar features. When, for example, 17 MeV Au^{+7} ions impinge in 200 nm GaSb films, S_e ∼3.1 keV/nm and S_n ∼1.4 keV/nm at the surface (as calculated by SRIM (Ziegler et al., 1985)), and these values are not very different at the interface. Hence, the modifications induced by ion irradiation with 17 MeV Au^{+7} ions may be due to a combination of nuclear and electronic energy losses.

Fig. 1 shows SEM micrographs of GaSb-sputt films, deposited on SiO_2/Si substrates at 400 °C, and the dramatic transformation induced by ion irradiation on those films. While as-deposited GaSb samples are compact, ∼200 nm thick, after irradiation with 1×10^{14} cm^{-2} the morphology of the films changes significantly, forming large voids separated by ∼25 nm thick walls. For 3×10^{14} cm^{-2} the voids increase even further, yielding an overall swelling of the films (Manzo et al., 2019). Similar effect is also observed in InSb-sputt films irradiated under similar conditions (Giulian et al., 2017b), although, for 75 nm thick InSb films, the swelling is more pronounced than that observed for GaSb (Manzo et al., 2019) or even InSb with thickness >100 nm (Giulian et al., 2017b). The reason for such different swelling relies on the initial structure of the films. While 200 nm thick GaSb or InSb films deposited by magnetron sputtering are polycrystalline, with zincblende phase, InSb films deposited by magnetron sputtering, at room temperature, with thickness 75 nm, are amorphous (Giulian et al., 2017b). The structural analysis of these films and its evolution upon ion irradiation is discussed in the next section.

Fig. 2 shows SEM micrographs of InSb-MBE films, with initial thickness of ∼370 nm, and the pronounced swelling induced by ion irradiation on those films can be readily seen. The morphology of InSb-MBE foams (Fig. 2) is very similar to that of GaSb-sputt foams (Fig. 1), and also to that of InSb-sputt (Giulian et al., 2017b). However, the same irradiation fluence yields quite distinct results for the swelling of InSb-sputt (75 nm thick) and InSb-MBE films irradiated with 2×10^{14} cm^{-2}, as shown in Fig. 3. For better visualization, Figs. 1 and 2 show SEM micrographs with the same scale (for a given material), irradiated with different fluences, so the relative increase in thickness can be directly appreciated,

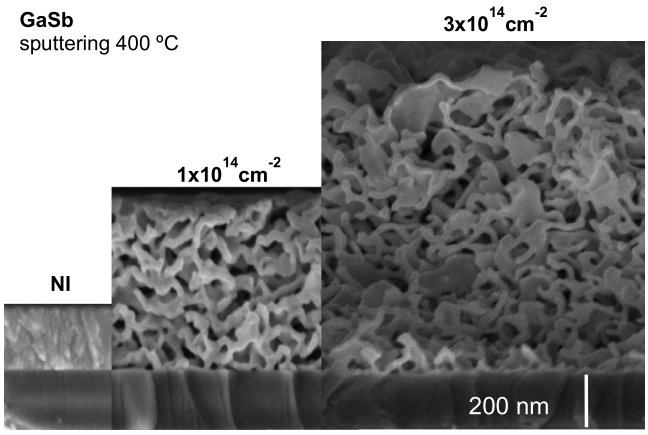

Fig. 1. SEM micrographs of GaSb films deposited by magnetron sputtering, before and after irradiation with 17 MeV Au^{+7} ions at different fluences (on scale).

while Fig. 3 shows two micrographs of samples irradiated with the same fluence (2×10^{14} cm^{-2}) but with different scales.

The swelling, for InSb-sputt, InSb-MBE and GaSb films is also plotted as a function of irradiation fluence in Fig. 4. While GaSb-sputt, InSb-sputt films (with initial thickness above 200 nm) and InSb-MBE exhibit similar swelling (approximately 5 times the initial film thickness for irradiation fluence of 3×10^{14} cm^{-2}), InSb-sputt films with initial thickness 75 nm exhibit a much more pronounced swelling, ∼16 times the initial film thickness for 3×10^{14} cm^{-2}. AlSb-sputt films, on the contrary, do not show any indication of voids or swelling upon irradiation under similar conditions (not shown). The SEM micrographs shown in Fig. 3 also emphasize the strikingly different behaviour of films with different initial structure. Bear in mind that InSb-sputt films are amorphous (before irradiation) (Giulian et al., 2017b) while InSb-MBE films are single crystalline.

With XRD analyses (Fig. 5), we could verify that not only the morphology of the film changes upon irradiation, but also the structure. As-deposited GaSb-sputt films are polycrystalline and, with increasing irradiation fluence, the well-defined peaks related to the zincblende phase of GaSb give place to broad peaks indicative of amorphization. At 1×10^{14} cm^{-2}, the zincblende phase can no longer be identified in GaSb-sputt samples (Manzo et al., 2019). Very interestingly, for InSb-sputt films, the opposite trend is observed. InSb films with thickness 75 nm, deposited by magnetron sputtering at room temperature, are amorphous, and upon irradiation with 17 MeV Au^{+7} ions, the structure of the films changes, attaining a zincblende phase for irradiation fluences of 1×10^{13} cm^{-2} and above (Giulian et al., 2019). AlSb-sputt films, 500 nm thick deposited at 550 °C, on the other hand, exhibit very good polycrystalline structure and do not show any significant structural changes upon irradiation with fluences as high as 2×10^{14} cm^{-2}, retaining the same zincblende phase exhibited by as-deposited films. Crystallite sizes of GaSb, InSb and AlSb samples determined using the Scherer equation (Patterson, 1939; Langford and Wilson, 1978) are listed in Table 1 (for a complete description of the calculation see Ref. Manzo et al., 2019).

Although in many of the III-V semiconductors ion irradiation induces amorphization (Schnohr, 2015), in amorphous InSb films (as shown in Fig. 5) the ion irradiation induces recrystallization (Giulian et al., 2017b). Similar behaviour can also be attained (in amorphous InSb films) by thermal annealing with temperatures as low as 150 °C, nonetheless, no evidence of porosity induced by thermal annealing was observed (Giulian et al., 2017b). The considerable difference in swelling between amorphous and polycrystalline InSb films irradiated under similar conditions may be attributed to the existing defects in amorphous films, which lower the energy required for vacancies and interstitials to move. It becomes evident from the XRD results shown in Fig. 5 that intrinsic thermodynamic properties of each compound play a significant role in ion-induced foams. AlSb is a semiconductor with bandgap ∼1.65 eV and melting temperature of 1057 °C, while GaSb and InSb melt at considerably lower temperatures (712 °C and 527 °C, respectively), besides having significantly smaller bandgaps (∼0.75 eV and ∼0.17 eV, respectively). Moreover, GaSb films deposited by magnetron sputtering at room temperature exhibit an excess Sb to the ratio 1:2 Ga:Sb, even though the sputtering target used for deposition consisted of 1:1 Ga:Sb (Giulian et al., 2019). Stoichiometric GaSb films were only attained when depositions were performed at elevated temperatures. In this sense, 420 °C was the lowest deposition temperature for which the GaSb films exhibited good polycrystalline quality, with no excess Sb (the excess Sb was verified by Rutherford backscattering spectrometry, as shown in detail in Ref. Manzo et al., 2019).

Table 1
Crystallite sizes for GaSb, InSb and AlSb films deposited by magnetron sputtering, before and after irradiation with 17 MeV Au^{+7} ions, calculated using the Scherrer equation Langford and Wilson (1978).

Fluence (cm^{-2})	GaSb (nm)	InSb (nm)	AlSb (nm)
NI	15.1 ± 1.5		24.6 ± 2.3
1×10^{12}	14.0 ± 1.5		
4×10^{12}	13.4 ± 1.4		
1×10^{13}	9.1 ± 0.4	7.8 ± 1.3	
1×10^{14}		7.8 ± 1.2	
2×10^{14}			25.2 ± 4.3
3×10^{14}		9.6 ± 1.1	

X-ray diffraction analysis of InSb-MBE films also reveal interesting aspects of the ion irradiation-induced transformations in antimonides. Fig. 6 shows diffraction patterns of InSb-MBE films before and after irradiation with 17 MeV Au^{+7} ions, in the fluence range $0-1 \times 10^{15}$ cm^{-2}. For the sake of clarity, the diffractograms were divided in three parts: Fig. 6(a) shows a highlight of the region where the peaks from the zincblende phases of InSb (111) and GaAs (111) appear; Fig. 6(b) shows the full length of the diffractogram for the InSb-MBE as-deposited film; and Fig. 6(c) shows a magnified view of the same graph (as in Fig. 6(b)) for selected irradiation fluences. The single-crystalline structure of InSb-MBE samples (as grown) becomes evident from Fig. 6(b), where a single narrow peak is visible at 2θ ∼32 degrees. Both the InSb and GaAs have zincblende structure, but with different lattice parameters, hence, the epitaxial growth of InSb film on GaAs substrate results in lattice distortion on the InSb film. Also visible from this graph is the (111) peak from zincblende phase of the GaAs substrate, at 2θ ∼28 degrees. For increasing irradiation fluences, the GaAs (111) peak gets broader and decreases in amplitude (Fig. 6(a)), consistent with the increase in structural damage at the substrate by the impinging ions. The peak corresponding to the InSb single-crystal phase also changes with increasing fluence, but it does not disappear as fast as the GaAs one. For 1×10^{14} cm^{-2}, the GaAs signal completely disappear and small voids start to appear in the SEM. At 2×10^{14} cm^{-2} the peaks corresponding to the zincblende phase of InSb start to appear, at the same time as voids start to coalesce and a porous structure can be readily seen in Figs. 2 and 3. For increasing fluences, the polycrystalline zincblende phase of InSb gets more prominent, similar to the observed for InSb-sputt films irradiated with same energy, but for much lower fluences (Fig. 5) (Giulian et al., 2017b).

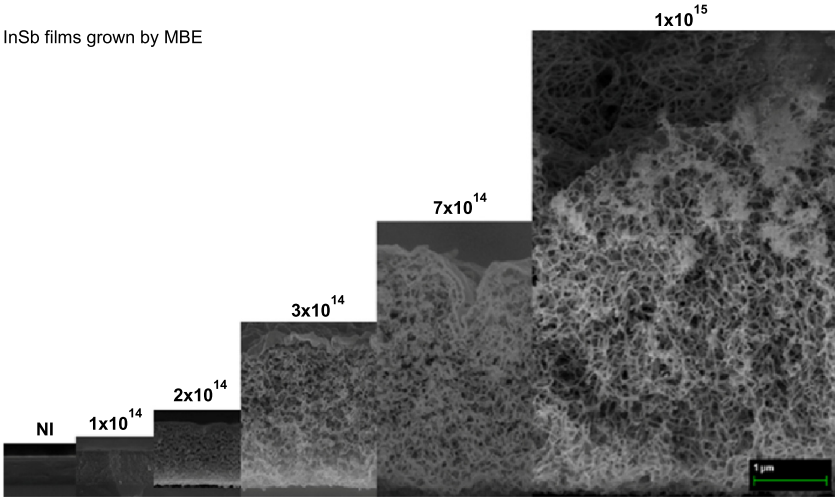

Fig. 2. SEM micrographs of InSb-MBE films, before and after irradiation with 17 MeV Au^{+7} ions at different fluences (on scale).

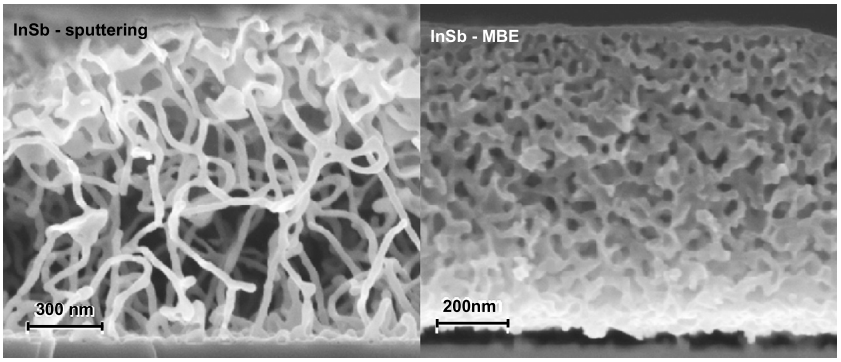

Fig. 3. SEM micrographs of InSb-sputt and InSb-MBE films, after irradiation with 17 MeV Au^{+7} ions to a total fluence of 2×10^{14} cm^{-2}. The thicknesses of the unirradiated films were 75 nm (InSb-sputt) and 370 nm (InSb-MBE), respectively.

The mechanisms responsible for the formation of voids in antimonides by ion irradiation is still a matter for debate, but a possible explanation follows Nitta et al. (2010), Kluth et al. (2006), Datta et al. (2014), Jacobi et al. (2012), Kluth et al. (2011) and Yanagida et al. (2017). Each ion creates a cylindrical region around its path where the mobility of atoms is enhanced by the local increase in temperature (Bierschenk et al., 2013; Kluth et al., 2014b; Ridgway et al., 2013). For a short time, vacancies and interstitials are highly mobile inside the molten (or vaporized) ion track, and diffuse away at different rates. Vacancies agglomerate forming voids which coalesce to minimize surface energy, while interstitials diffuse further away from the ion path. The foam-like structures shown in Figs. 1–3 most likely result from the coalescence of a large number of small voids formed by each individual impinging ion. The linear swelling with increasing irradiation fluence (Fig. 4) also supports that assumption. In this sense, the material behaves like a foam, where the nanowires shown in Figs. 1–3 are, in fact, the remaining plateau borders of a dry foam with open cell (Thomas et al., 2006). It is expected that amorphous films respond differently from polycrystalline ones upon irradiation, as confirmed by InSb and GaSb results (Giulian et al., 2017b, 2019). Polycrystalline films require more irradiation fluence to attain the same level of porosity observed for amorphous films of the same compound. InSb requires less energy to attain a polycrystalline structure than GaSb and AlSb, also, amorphous films can be transformed into foams by ion irradiation more easily than crystalline ones.

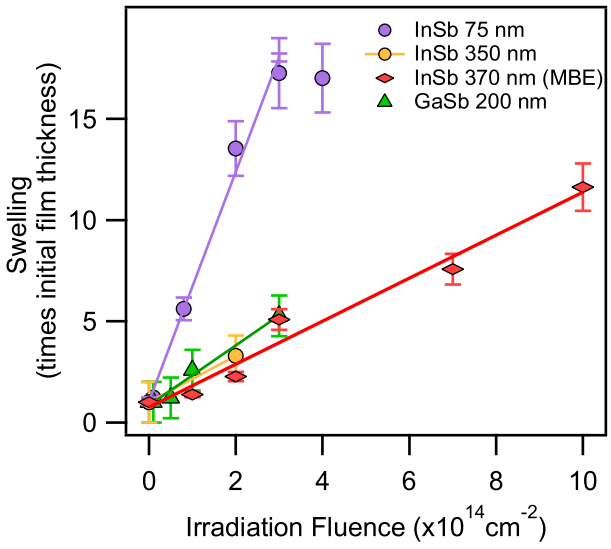

Fig. 4. Swelling as a function of irradiation fluence for InSb-sputt (300 nm initial thickness), InSb-sputt (75 nm initial thickness), GaSb-sputt and InSb-MBE films.

4. Electronic properties of InSb-MBE

Fig. 7(a) shows the mobility and electron density as a function of irradiation fluence for InSb-MBE films irradiated with 17 MeV

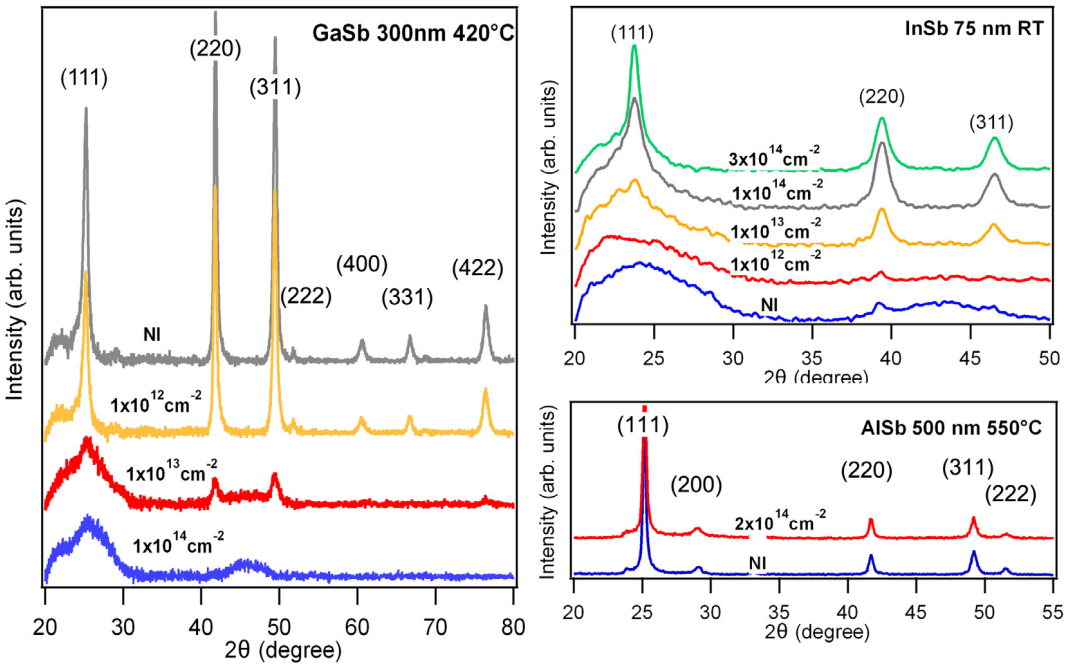

Fig. 5. GIXRD of GaSb-sputt, InSb-sputt (75 nm) and AlSb-sputt films as deposited and after irradiation with 17 MeV Au^{+7} ions. Diffractograms from samples irradiated with different fluences are vertically offset for clarity.

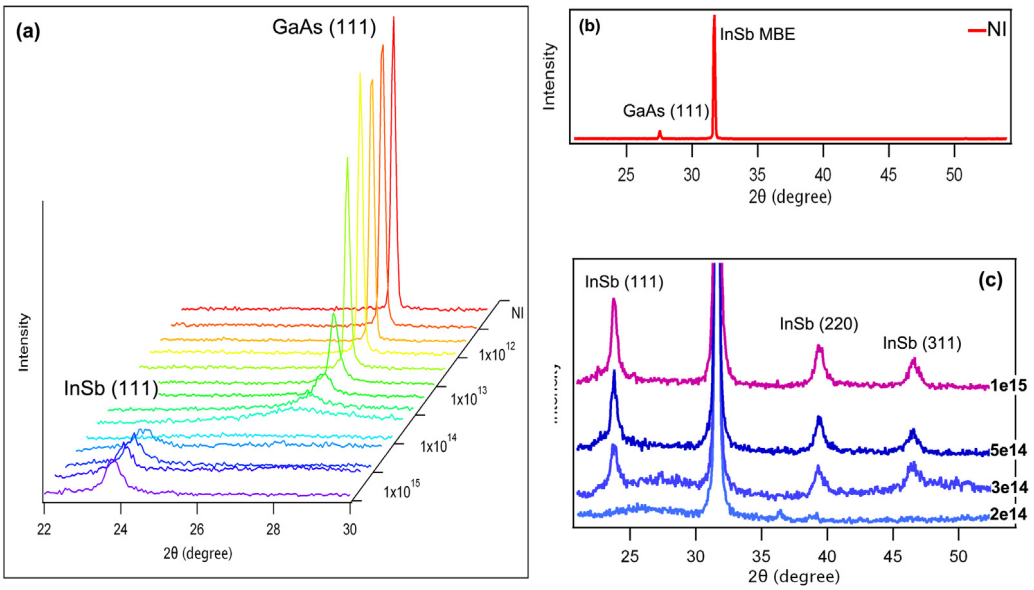

Fig. 6. XRD analysis of InSb-MBE films as-grown and after irradiation with different fluences. (a) Highlight of the region where the peaks from the zincblende phases of InSb (111) and GaAs (111) appear. Diffractograms shown in cascade for better visualization. (b) Diffractogram for the InSb-MBE as-grown film; (c) Magnified view of the same graph (as in Fig. 6(b)) for selected irradiation fluences, showing the formation of polycrystalline InSb with zincblende phase upon irradiation.

Au^{+7} ions, and Fig. 7(b) shows the mobility as a function of electron density for the same samples shown in Fig. 7(a). As Fig. 7(a) indicates, irradiation reduces the mobility. Saturation occurs for irradiation fluences higher than 3×10^{12} cm^{-2}. Notwithstanding, the electron mobility is increased by the irradiation and also shows the same pattern of saturation.

According to the Brooks–Herring model (Brooks, 1951), the mobility limited by ionized impurities is given by:

$$\mu \propto \frac{(T/T_0)^{3/2}}{n}\phi(n, T/T_0), \tag{1}$$

where T_0 is a reference temperature, and ϕ is a function that is nearly constant over the carrier concentration n. Therefore, the mobility due to ionized impurities is approximately inversely proportional to their concentration.

The mobility as a function of the electron density shown in Fig. 7(b) exhibits this trend. Thus, we conclude that the irradiation produces defects that limit the carrier motion, but these defects are ionized and work as dopants to the films. Moreover, the fitted mobility as a function of the carrier concentration is given by:

$$\mu = 2.10 \times 10^{16} \times N^{-1.03}, \tag{2}$$

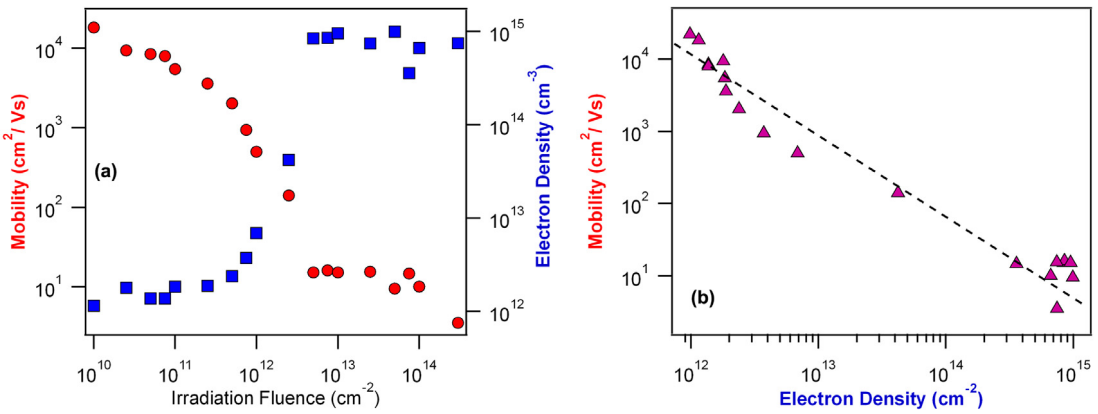

Fig. 7. (a) Mobility (red circles) and electron density (blue squares) as a function of irradiation fluence for InSb-MBE films irradiated with 17 MeV Au^{+7} ions. (b) Mobility as a function of electron density for the same samples shown in (a).

which is a good approximation for the Brooks–Herring model. Eq. (2) can also be written as:

$$\mu \sim 3.16 \times 10^{13} \left(\frac{T}{349}\right)^{3/2} \frac{1}{N^{1.03}} \tag{3}$$

Hence, we estimate a characteristic temperature T_0 of approximately 349 K for this scattering mechanism.

Conclusions

In this brief review we show that antimonide binary compounds can be transformed into solid foams with nanometric dimensions upon irradiation with 17 MeV Au^{+7} ions. The small bandgap of InSb and GaSb combined with the giant surface area of solid foams offer new possibilities for the development of energy efficient electronic and photonic devices. The results shown in this short review contribute to the understanding of antimonide binary thin film fabrication and structural characterization. We compare the ion irradiation effects on GaSb, InSb and AlSb films deposited by magnetron sputtering on SiO_2/Si substrates and InSb films epitaxially grown by MBE on GaAs. We show that GaSb-sputt films can be transformed from crystalline-to-amorphous and continuous-to-porous by ion irradiation. InSb-sputt films with thickness 75 nm can also be transformed into solid foams and they exhibit a much more pronounced swelling upon irradiation than single-crystalline InSb films or GaSb-sputt films irradiated under similar conditions. While polycrystalline GaSb-sputt films become amorphous upon irradiation, in amorphous InSb-sputt films the ion irradiation induces recrystallization. On the other hand, AlSb-sputt films do not show any significant structural changes or the formation of voids or swelling upon irradiation, retaining the same zincblende phase exhibited by as-deposited films. Significant structural transformations can also be seen in films irradiated with 17 MeV Au^{+7} ions. With increasing irradiation fluence, the InSb-MBE films also attain a polycrystalline structure, although the swelling of InSb-MBE films is significantly smaller than that of InSb-sputt (75 nm thick) for a given irradiation fluence, possibly due to the lower energy required for interstitials and vacancies to move in the amorphous film, compared to the crystalline one.

Acknowledgements

This work was financially supported by Conselho Nacional de Desenvolvimento Científico e Tecnológico (CNPq), Brazil and Fundação de Amparo à pesquisa do Rio Grande do Sul (FAPERGS), Brazil. The authors thank to the staff at the Laboratório de Conformação Nanométrica, Ion Implantation Laboratory and Centro de Microscopia e Microanálise at UFRGS and LNLS for their continued technical assistance.

References

Anandan, D., Nagarajan, V., Kakkerla, R.K., Yu, H.W., Ko, H.L., Singh, S.K., Lee, C.T., Chang, E.Y., 2019. Crystal phase control in self-catalyzed InSb nanowires using basic growth parameter V/III ratio. J. Cryst. Growth 522, 30–36.

Bierschenk, T., Giulian, R., Afra, B., Rodriguez, M.D., Schauries, D., Mudie, S., Pakarinen, O.H., Djurabekova, F., Nordlund, K., Osmani, O., Medvedev, N., Rethfeld, B., Ridgway, M.C., Kluth, P., 2013. Latent ion tracks in amorphous silicon. Phys. Rev. B 88.

Brooks, H., 1951. Scattering by ionized impurities in semiconductors. Phys. Rev. 83.

Cheng, Y., Yang, J., Jiang, Q., He, D., He, J., Luo, Y., Zhang, D., Zhou, Z., Ren, Y., Xin, J., 2017. New insight into InSb-based thermoelectric materials: from a divorced eutectic design to a remarkably high thermoelectric performance. J. Mater. Chem. A 5, 5163–5170.

Danilov, Y.A., Biryukov, A.A., Goncalves, J.L., Swart, J.W., Iikawa, F., Teschke, O., 2005. Photoluminescence and the Raman scattering in porous GaSb produced by ion implantation. Semiconductors 39, 132–135.

Datta, D.P., Kanjilal, A., Satpati, B., Dhara, S., Das, T.D., Kanjilal, D., Som, T., 2014. Argon-ion-induced formation of nanoporous GaSb layer: Microstructure, infrared luminescence, and vibrational properties. J. Appl. Phys. 116.

Datta, D.P., Som, T., 2016. Nanoporosity-induced superhydrophobicity and large antireflection in InSb. Appl. Phys. Lett. 108, 5.

Foll, H., Carstensen, J., Frey, S., 2005. Porous and Nanoporous Semiconductors and Emerging Applications, Vol. 2006. Spring Meeting of the Materials-Research-Society.

Giulian, R., Manzo, D.J., Bolzan, C.A., Bernardi, F., de Andrade, A.M.H., Schoffen, J.R., Baptista, D.L., 2019. Ion irradiation effects on Sb-rich GaSb films. Mater. Res. Express 6.

Giulian, R., Manzo, D.J., Salazar, J.B., Just, W., de Andrade, A.M.H., Schoffen, J.R., Niekraszewicz, L.A.B., Dias, J.F., Bernardi, F., 2017a. Structural and electronic characterization of antimonide films made by magnetron sputtering. J. Phys. D: Appl. Phys. 50.

Giulian, R., Salazar, J.B., Just, W., Manzo, D.J., de Andrade, A.M.H., Schoffen, J.R., Bernardi, F., Baptista, D.L., Fichtner, P.F.P., 2017b. Ion irradiation-induced polycrystalline InSb foam. J. Phys. D: Appl. Phys. 50.

Jacobi, C.C., Steinbach, T., Wesch, W., 2012. Development of porous structures in GaSb by ion irradiation. Nucl. Instrum. Methods Phys. Res. B 272, 326–329.

Kluth, S.M., Gerald, J.D.F., Ridgway, M.C., 2005. Ion-irradiation-induced porosity in GaSb. Appl. Phys. Lett. 86.

Kluth, P., Kluth, S.M., Johannessen, B., Glover, C.J., Foran, G.J., Ridgway, M.C., 2011. Extended x-ray absorption fine structure study of porous GaSb formed by ion implantation. J. Appl. Phys. 110.

Kluth, S.M., Llewellyn, D., Ridgway, M.C., 2006. Irradiation fluence dependent microstructural evolution of porous InSb. Nucl. Instrum. Methods B 242, 640–642.

Kluth, P., Sullivan, J., Li, W., Weed, R., Schnohr, C.S., Giulian, R., Araujo, L.L., Lei, W., Rodriguez, M.D., Afra, B., Bierschenk, T., Ewing, R.C., Ridgway, M.C., 2014a. Nano-porosity in GaSb induced by swift heavy ion irradiation. Appl. Phys. Lett. 104.

Kluth, P., Sullivan, J., Li, W., Weed, R., Schnohr, C., Giulian, R., Araujo, L.L., Lei, W., Rodriguez, M.D., Afra, B., Bierschenk, T., Ewing, R.C., Ridgway, M.C., 2014b. Nano-porosity in GaSb induced by swift heavy ion irradiation. Appl. Phys. Lett. 104.

Korotcenkov, G., Cho, B.K., 2010. Porous semiconductors: Advanced materials for gas sensor applications. Crit. Rev. Solid State Mater. Sci. 35, 1–37.

Langford, J.I., Wilson, A.J.C., 1978. Scherrer after 60 years - survey and some new results in determination of crystallite size. J. Appl. Crystallogr. 11, 102–113.

Manzo, D.J., Bolzan, C.A., Schoffen, J.R., de Andrade, A.M.H., Giulian, R., 2019. Structural and compositional analysis of GaSb nanofoams obtained by ion irradiation of sputtered films. Thin Solid Films 687.

Nitta, N., Hasegawa, T., Yasuda, H., Hayashi, Y., Yoshiie, T., Taniwaki, M., Mori, H., 2010. Void formation and structure change induced by heavy ion irradiation in GaSb and InSb. Mater. Trans. 51, 1059–1063.

Patterson, A.L., 1939. The scherrer formula for X-ray particle size determination. Phys. Rev. 56, 978–982.

Ridgway, M.C., Bierschenk, T., Giulian, R., Afra, B., Rodriguez, M.D., Araujo, L.L., Byrne, A.P., Kirby, N., Pakarinen, O.H., Djurabekova, F., Nordlund, K., Schleberger, M., Osmani, O., Medvedev, N., Rethfeld, B., Kluth, P., 2013. Tracks and voids in amorphous Ge induced by swift heavy-ion irradiation. Phys. Rev. Lett. 110.

Schnohr, C.S., 2015. Compound semiconductor alloys: From atomic-scale structure to bandgap bowing. Appl. Phys. Rev. 2.

Thomas, G.L., de Almeida, R.M.C., Graner, F., 2006. Coarsening of three-dimensional grains in crystals, or bubbles in dry foams, tends towards a universal, statistically scale-invariant regime. Phys. Rev. E 74, 021407.

Toulemonde, M., Dufour, C., Paumier, E., 2006. The ion-matter interaction with swift heavy ions in the light of inelastic thermal spike model. Acta Phys. Pol. A 109, 311–322.

Vurgaftman, I., Meyer, J.R., Ram-Mohan, L.R., 2001. Band parameters for III-V compound semiconductors and their alloys. J. Appl. Phys. 89, 5815–5875.

Yanagida, Y., Oishi, T., Miyaji, T., Watanabe, C., Nitta, N., 2017. Nanoporous structure formation in GaSb, InSb, and Ge by ion beam irradiation under controlled point defect creation conditions. Nanomaterials 7.

Ziegler, J.F., Biersack, J.P., Littmark, U., 1985. The Stopping and Range of Ions in Solids. Pergamon Press, New York.